



**HAL**  
open science

## Tuning of Structural and Optical Properties of Graphene/ZnO Nanolaminates

Margarita Baitimirova, Roman Viter, Jana Andzane, Arie van Der Lee, Damien Voiry, Igor Iatsunskyi, Emerson Coy, Lina Mikoliunaite, Saulius Tumenas, Karol Załęski, et al.

► **To cite this version:**

Margarita Baitimirova, Roman Viter, Jana Andzane, Arie van Der Lee, Damien Voiry, et al.. Tuning of Structural and Optical Properties of Graphene/ZnO Nanolaminates. *Journal of Physical Chemistry C*, 2016, 120 (41), pp.23716 - 23725. 10.1021/acs.jpcc.6b07221 . hal-01681269

**HAL Id: hal-01681269**

**<https://hal.umontpellier.fr/hal-01681269>**

Submitted on 12 Jul 2021

**HAL** is a multi-disciplinary open access archive for the deposit and dissemination of scientific research documents, whether they are published or not. The documents may come from teaching and research institutions in France or abroad, or from public or private research centers.

L'archive ouverte pluridisciplinaire **HAL**, est destinée au dépôt et à la diffusion de documents scientifiques de niveau recherche, publiés ou non, émanant des établissements d'enseignement et de recherche français ou étrangers, des laboratoires publics ou privés.

# Tuning of Structural and Optical Properties of Graphene/ZnO Nanolaminates

*Margarita Baitimirova<sup>1</sup>, Roman Viter<sup>2,3</sup>, Jana Andzane<sup>1</sup>, Arie van der Lee<sup>4</sup>, Damien Voiry<sup>4</sup>, Igor Iatsunskiy<sup>5</sup>, Emerson Coy<sup>5</sup>, Lina Mikoliunaite<sup>3,6</sup>, Saulius Tumenas<sup>3</sup>, Karol Załęski<sup>5</sup>, Zigmas Balevicius<sup>3</sup>, Ieva Baleviciute<sup>3,6</sup>, Almira Ramanaviciene<sup>3,6</sup>, Arunas Ramanavicius<sup>3,6</sup>, Stefan Jurga<sup>5</sup>, Donats Erts<sup>1\*</sup>, Mikhael Bechelany<sup>4\*</sup>*

<sup>1</sup>Institute of Chemical Physics, University of Latvia, 19 Raina Blvd., LV 1586, Riga, Latvia

<sup>2</sup>Institute of Atomic Physics and Spectroscopy, University of Latvia, 19 Raina Blvd., LV 1586, Riga, Latvia

<sup>3</sup>State Research Institute Center for Physical Sciences and Technology, Savanoriuave. 231, LT-01108, Vilnius, Lithuania

<sup>4</sup>European Institute of Membranes, University of Montpellier, Place Eugene Bataillon, 34095, Montpellier, France

<sup>5</sup>NanoBioMedical Centre, Adam Mickiewicz University, 85 Umultowska str., 61-614, Poznan, Poland

<sup>6</sup>Faculty of Chemistry, Vilnius University, 24 Naugarduko, LT-03225, Vilnius, Lithuania

\* Corresponding author : mikhael.bechelany@univ-montp2.fr, Phone: +33467149167, Fax: +33467149119

DonatsErts: donats.erts@lu.lv

## ABSTRACT

Zinc Oxide (ZnO) and graphene (G) have been extensively studied because of their unique physical properties. Here, Graphene-Zinc Oxide (G/ZnO) nanolaminates were fabricated, respectively,

by chemical vapor deposition and low temperature atomic layer deposition technique. The number of obtained G/ZnO layers was tuned from 1 to 11 with a total thickness of 100 nm for all prepared nanolaminates. The structure, optical properties and interaction between G and ZnO were studied by X-ray methods, TEM, AFM, Raman and optical spectroscopy. The obtained results were interpreted and analysed taking into account strain and charge effects of graphene in G/ZnO nanostructures. We demonstrate that the bottom graphene used as a substrate stimulated the formation of ZnO crystalline structure. n-doping of graphene caused by charge transfer from ZnO to graphene has been detected by blue-shift of G-band of Raman spectra of the nanolaminates. ZnO photoluminescence intensity was found to be dependent on the number of graphene layers in G/ZnO nanolaminate. n-doping of graphene could be tailored by controlling the construction of the G/ZnO nanolaminates for variety of applications such as, for example, selective adsorption of the target molecules on graphene surface. Thus, G/ZnO nanolaminates may find applications in optical, bio- and chemical sensors.

## INTRODUCTION

In the past few years both semiconductors – zinc oxide (ZnO) and graphene (G, semiconductor with zero eV band gap) have been extensively studied because of their unique physical properties. ZnO is known as n-type semiconductor with good transparency, high electron mobility, wide band gap of 3.37 eV, high exciton binding energy of 60 meV and strong luminescence at room temperature.<sup>1, 2</sup> Due to high photo-sensitivity, chemical stability and non-toxicity, ZnO is perspective material for application in UV<sup>3</sup>, gas<sup>4, 5</sup> and biological sensors.<sup>6, 7</sup>

The sensitivity of ZnO can be enhanced not only by the decrease of its dimensions down to nanostructures,<sup>8</sup> but also by its combination with carbon-based nanomaterials (carbon nanotubes, graphene) in composites and hybrid structures.<sup>9, 10</sup> Investigations of single graphene-ZnO interfaces showed that graphene can act as an excellent electron acceptor and transport material for effectively separate photoinduced excitons formed in ZnO.<sup>11, 12</sup> This property makes the combination of graphene-ZnO highly promising for applications in optoelectronic devices,<sup>11, 13</sup> gas<sup>14</sup> and biological sensors,<sup>12, 14</sup> where graphene can act like a high conducting mesh. In its turn, sensor performance strongly depends on resistance of junction interface.<sup>15</sup>

ZnO thin films can be synthesized using various methods including hydrothermal,<sup>16</sup> Chemical Vapor Deposition (CVD),<sup>17</sup> magnetron and RF sputtering,<sup>18, 19</sup> spin-coating,<sup>20</sup> ultrasonic spray pyrolysis<sup>21</sup> and atomic layer deposition (ALD)<sup>21-23</sup> methods. Among these methods, ALD enables the deposition of high quality and uniform thin films with controlled reaction and growth mechanism at the atomic level and performed at low temperatures (60-100 °C).<sup>22-24</sup> We note here that the ability to synthesize ultrathin film at low temperature offered by ALD is important to prevent the interdiffusion of materials.<sup>24</sup>

Graphene can be fabricated by exfoliation from graphite,<sup>25</sup> reduction of exfoliated graphene oxide,<sup>26</sup> epitaxial growth using SiC substrates<sup>27</sup> and CVD on a metal catalytic layer (Cu, Ni).<sup>28</sup> Due to economic feasibility and easy fabrication, exfoliated graphene and exfoliated reduced graphene oxide have mostly been used for the fabrication of graphene-ZnO heterostructures.<sup>13, 14, 16, 28, 29</sup> However, the

exfoliation method produces graphene layers with uncontrollable number of monolayers, limited area of coating and poor electronic properties. On the contrary, the CVD method enables the production of high quality monolayer graphene films with large continuous areas and allows as well the transfer of graphene sheets on arbitrary substrates. In a previous report on graphene-ZnO hybrid structures, CVD graphene was used either as a substrate for ZnO deposition, *i.e.*, as a bottom layer,<sup>30</sup> or as a top layer.<sup>31</sup> To our knowledge, the design of hybrid material composed of “graphene at the bottom and on the top of ZnO layer”, as well as multilayer graphene-ZnO “sandwich”-type nanostructures (G/ZnO nanolaminates) have not been reported yet. Similarly to previously reported Al<sub>2</sub>O<sub>3</sub>/ZnO nanolaminates,<sup>32</sup> where Al<sub>2</sub>O<sub>3</sub> layers affected the band gap and photoluminescence of ZnO, influence of graphene on ZnO properties (crystal growth, photoluminescence and band gap), as well as influence of ZnO on graphene properties (strain, charging) are expected in G/ZnO nanolaminates.

In this study the G/ZnO nanolaminates were fabricated by creating alternating ZnO and graphene layers with total nanolaminate thicknesses of 100 nm, which enables structural and optical measurements well above the noise level.<sup>23</sup> The fabrication of nanostructures started with the graphene as a bottom layer of a nanolaminate, promoting formation of hexagonal wurtzite structure of ZnO from its first deposited atomic layers. In the next steps ZnO interlayers of different thicknesses were alternated with graphene monolayers. The graphene was chosen also as a top layer of the nanolaminate as it is compatible with most organics, bio- and gas molecules. Therefore, fabricated G/ZnO nanolaminates offer perspective for wide range of applications such as optoelectronic devices, sensors and catalysts.

## MATERIALS AND METHODS

G/ZnO nanolaminates were deposited on Si substrates with native silicon oxide (SiO<sub>2</sub>) layer. The Si/SiO<sub>2</sub> substrates were ultrasonically pre-cleaned with acetone, ethanol and deionized water for 15 min. Monolayer graphene films were synthesized by copper-catalysed low-pressure CVD as reported elsewhere<sup>33</sup> using a reactor (First Nano Easy tube 101). Graphene monolayers were

transferred to the desired substrate by polymer-assisted transfer technique<sup>34</sup> followed by the deposition of ZnO layer over it (Figure 1). ZnO layers of the thickness of 10, 25, 50 and 100 nm were synthesized by ALD method using home-made ALD reactor<sup>35</sup> at the same conditions as described elsewhere.<sup>23</sup> In the next step, graphene monolayer was transferred onto the deposited ZnO layer. The sequential deposition of ZnO layer and graphene transfer was repeated until multilayer structure with a total thickness of 100 nm was obtained. For the comparison, 100 nm thick pure ZnO thin film was deposited on Si substrate using the same ALD conditions. Further in the text the samples are named by the formula  $G_{xL}ZnO_{ym}$ , where  $x$  is the number of graphene layers and  $y$  is the thickness in nanometers of ZnO single layer in multilayer structure.

The surface topography of fabricated G/ZnO nanolaminates was characterized using atomic force microscopy (AFM, Asylum 3D). The morphology and structure of G/ZnO nanolaminates were studied by X-ray reflectivity (XRR, Bruker D5000), X-ray diffraction (XRD, Bruker D5000 with  $CuK\alpha$  radiation, using the Bragg-Brentano symmetric configuration) and high-resolution transmission electron microscopy (HRTEM, JEOL ARM 200F (200 kV)). The cross sections and lamellas for TEM investigations were prepared by focused ion beam milling (JEOL JIB-4000) by the method described elsewhere.<sup>36</sup> The Raman spectra were obtained using Witek ALFA300R Raman spectrometer with 532 nm excitation laser source. Optical properties of G/ZnO nanolaminates were analyzed by UV-VIS reflectance (Shimadzu UV-3600) and photoluminescence (Edinburg Instruments FLS 980) spectroscopy. The excitation of luminescence was performed by a Xe lamp line, centred at 280 nm. The band gap of ZnO was calculated in absorption edge region according to the procedure, described elsewhere.<sup>37</sup>

## RESULTS AND DISCUSSION

In order to understand the effect of graphene incorporation on G/ZnO properties, G/ZnO nanolaminates were fabricated by alternating ZnO and graphene layers with total nanolaminate thickness of 100 nm. The fabrication of nanostructures started with graphene as

a bottom layer of the nanolaminate. In the next steps ZnO interlayers of different thicknesses were alternated with graphene monolayers. Graphene was chosen also as a top layer of the nanolaminate (**Figure 1**). The samples are named by the formula  $G_{xL}ZnO_{ym}$ , where  $x$  is number of graphene layers and  $y$  is the thickness in nanometers of ZnO single layer in multilayer structure.

High-resolution cross-section TEM images confirmed the sequence of alternating ZnO and graphene layers throughout all fabricated nanolaminates (**Figure 2 a-d**). The native silicon oxide ( $SiO_2$ ) layer on the silicon surface was about 2 nm thick (Figure 2a inset). The total thickness of all obtained G/ZnO nanolaminates was about 100 nm. From TEM images, it can be seen that the individual ZnO layers were of constant thickness and well reproducible. However, the increase of a number of graphene interlayers and accordingly decrease of ZnO interlayer thickness results in worsening of layers smoothness (Figure 2 c, d), most likely related to increase of nanolaminate surface roughness.

The high resolution TEM analysis of G/ZnO nanolaminates showed the presence of (100), (002), (101), (110) and (103) fringes in the selected area of ZnO layer (Figure 2 e, f). The fringe separation of 0.275 nm determined from the HRTEM image (Figure 2 e) corresponds to (100) plane of wurtzite crystal structure of ZnO.

Obtained XRD spectra of the ZnO layers of G/ZnO nanolaminates (**Figure 3 a**) demonstrated the diffraction peaks at  $2\theta = 31.80^\circ$ ,  $34.54^\circ$ ,  $36.16^\circ$  and  $56.32^\circ$ , corresponding to (100), (002), (101) and (110) reflection planes of hexagonal wurtzite structure of ZnO respectively<sup>8</sup> in perfect agreement with TEM results. The peak related to (103) plane of ZnO crystal presented in FFT image (Figure 2 f) was not observed as it was out of XRD measurement range (diffraction peak position of (103) plane is at  $2\theta = 62.7^\circ$ ).<sup>38</sup> Peak observed at  $2\theta = 32.95^\circ$  is corresponding to (004) reflection plane of silicon substrate.

The above peaks were observed in XRD patterns of all G/ZnO nanolaminates, indicating their high crystalline structure. No characteristic peaks for any impurities as, for example, PMMA, FeCl<sub>3</sub>, Cu, etc. residuals from graphene transfer process, were observed. Calculated from XRD spectra ZnO lattice constants were equal to  $a = 0.325$  nm and  $c = 0.519$  nm, which fits perfectly with ZnO crystal lattice parameters.<sup>38</sup> The lattice spacing between the atom stacks calculated from the FFT image of a selected area of ZnO interlayer were in good correlation with XRD data (Figure 2f (inset) and Figure 3a). No significant changes of ZnO lattice parameters were observed with decreasing of thickness of ZnO interlayers in the nanolaminates, which is in good correlation with previous report on lattice parameters of ALD deposited ZnO thin films of different thicknesses.<sup>23</sup>

No amorphous-to-crystalline growth transition of ZnO was observed in contradiction with previously reported ALD deposited on Si/SiO<sub>2</sub> substrates ZnO thin films<sup>23</sup> and Al<sub>2</sub>O<sub>3</sub>/ZnO nanolaminates,<sup>32</sup> where the amorphous-to-crystalline transition of ZnO occurred for the layers with thickness larger than 25 nm and 10 nm respectively. As it can be seen from the obtained G/ZnO nanolaminates XRD and HRTEM data, even the thinnest (10 nm) ZnO layers have a crystalline nature (Figure 3, G<sub>11L</sub>ZnO<sub>10nm</sub>, Figure 2f).

From the intensities of the diffraction peaks in XRD spectra (Figure 3a, b) it can be seen that for the 10 and 25 nm thick ZnO interlayers, the [002] crystal growth direction is dominating, while with an increase of ZnO interlayer thickness up to 50 nm, as well as for the 100 nm thick ZnO thin film deposited on Si/SiO<sub>2</sub> substrate, the [100] and [101] growth directions significantly dominate over [002] and [110] directions. Presumably, the graphene sublayers promote growth of ZnO crystalline transition layer in [002] direction, which is attributed to very low (< 3%) mismatch between the graphene and the ZnO (002) hexagonal lattices.<sup>39</sup> With the increase of ZnO interlayer thickness, [100] and [101], considered as fast



ZnO growing directions are prevailing.<sup>39</sup> These results suggest that the advantageous role of graphene as template in the formation of highly crystalline ZnO.

The AFM images of the surface of 100 nm thick G/ZnO nanolaminates with various numbers of graphene interlayers indicate that as the number of graphene interlayers increases, the morphology of the top graphene surface became rougher (**Figure 4a,b**). The calculated root mean square (RMS) roughness of the surface of G/ZnO nanolaminates from AFM data showed linear increase versus the number of graphene layers in the nanolaminates (Figure 4 c). The explanation may be related to the fact that every next graphene layer follows the morphology of the ZnO sublayer surface. The RMS estimation does not account for possible artifacts (strain/elastic resistance of graphene) that might be caused by the pressure of AFM probe during the surface scanning.

The increase of the surface roughness of the G/ZnO nanolaminates as determined is supported by the X-ray reflectivity data (**Figure 5**). In comparison with pure ZnO thin film ( $G_{0L}ZnO_{100nm}$ ), the number of Kiessig fringes was significantly reduced when increasing number of graphene layers ( $G_{2L}ZnO_{100nm}$ ,  $G_{3L}ZnO_{50nm}$ ,  $G_{5L}ZnO_{25nm}$ ) and then disappeared for  $G_{11L}ZnO_{10nm}$ , indicating an increase of the G/ZnO nanolaminate surface roughness as well as the interfacial roughness. The ZnO layer without any graphene top or bottom layer ( $G_{0L}ZnO_{100nm}$ ) showed nearly perfect Kiessig fringes, which can be modelled using Parrat's recursive formula<sup>40</sup> for X-ray reflectivity. The thickness of ZnO layer calculated from the Kiessig fringes was 99.7 nm in perfect agreement with the TEM data. The surface roughness of 1.6 nm was rather close to the RMS surface roughness of 1.9 nm, which was determined by AFM. The gradual extinction of the Kiessig fringes, which is apart from the rather large surface roughness, for larger incident angles— is also observed due to the roughness at the buried interface between the substrate and the film (0.8 nm).

We note here that due to the gas barrier properties of the graphene CVD thin films,<sup>41</sup> the porosity of our thin films could not be evaluated using common techniques such as Surface acoustic wave (SAW) /BET technique or Ellipsometry Porosimetry.

The reflectivity curve of G/ZnO nanolaminates with two graphene layers  $G_{2L}ZnO_{100nm}$  showed some short-period Kiessig fringes at very small angles due to the thickness of the ZnO layer and a long-period fringe with a (first) minimum at  $2\theta = 0.9$ . Although these long-period Kiessig fringes at very small angles could be attributed to the bottom graphene layer, they are more coming from the native silica layer of the substrate (Figure 5). The same long-period fringe was seen slightly shifted to larger angles in the reflectivity curve of nanostructures with three graphene layers  $G_{3L}ZnO_{50nm}$ . The fringes between  $2\theta=0.5-0.9^\circ$  correspond to the 50 nm thick ZnO interlayers and fringes below  $2\theta = 0.5^\circ$  appeared due to the total thickness of the G/ZnO multilayer nanostructure. The reflectivity curve of G/ZnO nanostructures with five graphene layers  $G_{5L}ZnO_{25nm}$  showed different fringe periodicities and did not allow to identify the thickness of ZnO interlayers. The reflectivity curve of G/ZnO nanostructures with eleven graphene layers  $G_{11L}ZnO_{10nm}$  cannot be interpreted qualitatively or quantitatively because of its very high RMS surface roughness (Figure 4).

The top graphene layer cannot be detected in the reflectivity curves, because the RMS surface roughness of G/ZnO nanolaminates is much larger than the supposed thickness of the graphene layer. Additionally it is worth noting that because of the quenching of the Kiessig fringes, caused by the relatively high surface and interfacial roughness of G/ZnO nanolaminates, the reflectivity curves of all fabricated G/ZnO structures cannot be analyzed quantitatively, but only qualitatively.

In order to evaluate possible strain and charging effects of graphene in G/ZnO nanolaminates, the Raman spectra of the fabricated structures were investigated (**Figure 6a**).

Two intensive peaks at  $1583\text{ cm}^{-1}$  and  $2671\text{ cm}^{-1}$ , corresponding to the G band induced by the vibration of  $\text{sp}^2$ -hybridized carbons and to the 2D band of second-order process induced Raman feature, respectively,<sup>42</sup> were observed in all the obtained spectra of the G/ZnO nanolaminates. Both G and 2D peaks were sharp, indicating that no oxidation of graphene to graphene oxide<sup>43</sup> occurred during the formation of ALD ZnO layers and thus suggesting that the high quality of graphene is largely preserved.

The ratio of intensities of the 2D band to the G band ( $I_{2D}/I_G$ ) of single CVD graphene layers used for the G/ZnO nanolaminates fabrication was above 2 (see **Table 1**,  $G_{1L}ZnO_{0nm}$ ), confirming the monolayer structure of this graphene.<sup>44</sup> The observed low intensity of D peak at  $1350\text{ cm}^{-1}$  in this spectrum (Figure 6a, Table 1) indicated the presence of insignificant amount of structural defects in the monolayer, which is typical for CVD-grown on Cu substrate graphene.<sup>45</sup> When increasing the number of graphene interlayers in the nanolaminates, the  $I_D/I_G$  ratio moderately increased from 0.1 for a single graphene monolayer up to  $\sim 0.22$  for the G/ZnO nanolaminates containing from 2 to 11 graphene layers regardless the number of the graphene layers in the nanolaminate (Table 1). Thereby, in contradiction with sputtering techniques, where significant increase in the  $I_D/I_G$  peak intensity ratio up to 1 is typically observed after ZnO deposition on the graphene substrate,<sup>46</sup> the ALD deposition of the ZnO on graphene surface does not induce severe structural damage in it.

The  $I_{2D}/I_G$  ratio in the Raman spectra of G/ZnO nanolaminates decreased from 2.68 for the nanolaminate containing two graphene layers  $G_{2L}ZnO_{100nm}$  down to 1.33 and 1.20 for  $G_{3L}ZnO_{50nm}$  and  $G_{5L}ZnO_{25nm}$  structures containing 3 and 5 graphene layers, respectively, and further down to 0.87 for the  $G_{11L}ZnO_{10nm}$  nanolaminate containing 11 graphene layers (Figure 6 a-c, Table 1). These changes in  $I_{2D}/I_G$  intensity ratio may be related to such processes occurring in graphene layers of nanolaminates as charging<sup>47</sup> and/or mechanically induced strain.<sup>48</sup> However, the typical redshifts for uniaxial or biaxial graphene strain of either G or

2D peaks by  $30\text{-}50\text{ cm}^{-1}$  per 0.5% of strain<sup>48</sup> were not observed. This suggests that graphene interlayers in the G/ZnO nanolaminates do not experience significant strain, and the changes in positions and intensity ratios of G and 2D peaks are mostly related to graphene charging. In spite of absence of the significant damage, the minor strain of graphene may take place in G/ZnO nanolaminates. The first layer of graphene of all prepared structures may have insignificant strain due to van der Waals interaction between the graphene and silicon substrate during transfer. The next transferred graphene layers of G/ZnO nanolaminates may be exposed to strain forming from van der Waals force existing at the graphene-ZnO (002) interface of ZnO-graphene hybrid structures<sup>39</sup> that may result in graphene strain due to lattices mismatch, as well as to the increase of roughness of the nanolaminates (Figure 4).

The evaluation of G-band position of nanolaminates showed that it blue-shifts with the increase of number of graphene interlayers and respectively decreases of thickness of ZnO interlayers (Figure 6 a,b,c). Blue-shift of G-band is indicative for the graphene charge.<sup>49</sup> As in ZnO-graphene hybrid structures, the electron transfer occurs from ZnO to graphene as a result of the difference in their work functions,<sup>39</sup> the above changes in Raman spectra of G/ZnO nanolaminates may be attributed to the negative charge of graphene by electron transfer from ZnO layer. Presumably, this electron transfer from ZnO to graphene results in the formation of depletion layer in ZnO near the graphene surface, and facilitates accumulation of holes in it. For quantifying graphene charge in the G/ZnO nanolaminates, the estimation of concentration of excess electrons per graphene layer was performed based on data reported on interdependence between Raman shift of G-band and the increase of concentration of electrons in monolayer graphene.<sup>47</sup> It was found that the charge per graphene layer linearly decreases with the increase of number of graphene layers and respectively with decrease of thickness of ZnO interlayers (Figure 6 c). The reason for graphene charge to decrease may be related to the interaction and the overlapping of ZnO depletion layers with the decrease of

ZnO interlayer thickness, as well as to the change of defect concentration in ZnO interlayers related to change of prevailing crystallographic ZnO growth directions with the decrease of interlayer thickness (Figure 3), and requires further clarification. However, this linear dependence of graphene charge on number of graphene layers in G/ZnO nanolaminates may be useful in charge-related applications, for example, for tuning graphene charge by varying the number of graphene interlayers in the nanolaminates for selective adsorption of positive charged target molecules on the graphene surface.

The number of graphene interlayers and thickness of ZnO layers in G/ZnO nanolaminates has strong influences on their optical properties. The shift of ZnO absorption edges from 360 up to 400 nm is clearly seen on reflectance spectra recorded for different G/ZnO nanolaminates (**Figure 7a**). The shift of absorption edges of G/ZnO nanolaminates relative to absorption edge position of pure ZnO may be related to the formation of optically active defects at the graphene-ZnO interface<sup>50</sup> and ZnO grain boundaries. The band gap of G/ZnO nanolaminates was calculated from the assumption that the reflectance in the absorption edge is related to the band gap values due to the following equations<sup>23</sup>:

$$D = \ln\left(\frac{100}{R}\right)$$

$$(D \cdot hv)^2 \sim (hv - E_g)$$

Where R, D, hv and E<sub>g</sub> are reflectance, optical density, photon energy and band gap, respectively. The E<sub>g</sub> values were calculated from the intersection of linear part of the curve with hv-axis. The fitting was performed automatically using Origin 7.0 software (Figure 7b). The obtained band gap values determined from the reflectance spectra of ZnO decrease with the increase of the number of graphene interlayers and the decrease of thickness of ZnO interlayers in nanolaminates from the initial value of 3.42 eV, obtained for pure ZnO thin film, down to value of 3.10-3.13 eV for nanolaminates containing 5 and more graphene layers

respectively (Figure 7c). The levelling of the band gap at these values may be related to the domination of ZnO [002] crystallographic growth direction over other directions at ZnO interlayer thicknesses below 25 nm as confirmed by XRD data (Figure 3), which may reduce the concentration of optically active defects.

In the photoluminescence (PL) spectra of G/ZnO nanolaminates (**Figure 8a**), the peaks with maximum at ~3.3 eV (375 nm) related to excitation transitions in ZnO<sup>8, 23</sup> were observed for all samples. Peaks related to deep level transitions at energies about 2.4 - 2.5 eV (oxygen and zinc vacancies and zinc interstitials),<sup>51</sup> as well as at 2.0 eV, related to interstitial oxygen in ZnO films<sup>51</sup> were not observed for both ZnO thin film deposited on SiO<sub>2</sub> surface and for G/ZnO nanolaminates. From the Figure 8 it is clearly seen that the intensity of PL signals decreased with the increase of number of graphene layers and the corresponding decrease of the thickness of ZnO interlayers in the G/ZnO nanolaminates. PL emission may be quenched because of several reasons such as negative charge of graphene surface, with concomitant screening effect in graphene,<sup>52</sup> transfer and trapping of photo-excited electrons in graphene,<sup>11, 12, 39</sup> and similarly to ZnO/Al<sub>2</sub>O<sub>3</sub> nanolaminates the increase of the total depletion regions relative to total thickness of ZnO (100 nm) when decreasing the ZnO layer thickness<sup>32, 50</sup>. These factors result in the decrease of exciton radiative recombination compared to non-radiative processes in the G/ZnO nanolaminates with the increase of the number of graphene interlayers and the decrease of thickness of ZnO interlayers. The presumable thickness of ZnO layer with 100%-quenched PL near the single surface of a graphene interlayer was estimated by empirical linearization of PL luminescence intensity as function of summed all quenched ZnO layer thicknesses in the G/ZnO nanolaminates. The closest to linear curve was obtained assuming that the thickness of a ZnO layer with quenched PL was 10 nm near every graphene/ZnO interface (Figure 8 b). However, as it can be seen from the Figure 8 a-b, PL signals are still detected when the presumed total thickness of ZnO layers in between two

graphene layers is 10 nm (Figure 8 b, point  $G_{11L}ZnO_{10nm}$ ). As a consequence, it can be concluded that PL quenching mechanism in the nanolaminates may not be only based on the dimension of architecture and thus a more complex model is required to fully understand the optical properties of such graphene/ZnO layered films.

## CONCLUSION

In summary, new nanomaterials of G/ZnO nanolaminates have been developed and investigated. Combination of CVD and ALD offers a precise control of the thickness and composition of the films. The number of alternating graphene and ZnO interlayers and the thickness of ZnO interlayers influenced the structure and the optical properties of the fabricated nanolaminates. During the ALD deposition of ZnO nanolayers, the bottom graphene used as a substrate stimulated the formation of ZnO crystalline structure, thus avoiding formation of amorphous transition layer between the graphene and the crystalline ZnO thin film.<sup>32, 50, 53,54</sup> We found that ALD deposition of ZnO thin films on surface of graphene layers did not introduce severe structural damage. Minor strain and charge transfer from ZnO to graphene were observed in fabricated G/ZnO nanolaminates. The charge transfer resulted in negative charging of graphene as observed by blue-shift of G-band of Raman spectra of the nanolaminates. These results are meaningful for exploration of devices based on Graphene and ZnO films and the conclusion obtained in this study could be commonly used for other Graphene/metal oxide nanolaminates. The ZnO PL intensity was found to be dependent on the number of graphene layers in G/ZnO nanolaminate. Presumably, the underlying reason for the PL decrease is the partial suppression of radiative recombination occurring at graphene-ZnO interface. The tuning of the graphene charge together with the ZnO PL intensity in G/ZnO nanolaminates has prospects in applications for FET gate,

biosensors, chemical sensors and catalysts. The variable negative charging of graphene layers might provide a selective adsorption of the positive charged target molecules on its surface. Optical properties of G/ZnO nanolaminates can be used in optical transducer during sensor/biosensor development. Finally, multilayer structure synthesized by alternating graphene and metal oxide layers could be very attractive for a wide range of applications such as the realization of mid-infrared graphene hyperbolic metamaterials,<sup>55</sup> encapsulation materials with high impermeability to moisture and air<sup>56</sup> or to improve the thermal conductivity of polymers.<sup>57</sup> These new properties of the G/ZnO nanolaminates materials are under investigations.

**ACKNOWLEDGEMENTS:**This work was supported by Latvian National Research program IMIS-2 and partially supported by the EU under BIOSENSORS-AGRICULT, Contract PIRSES-GA-2012-318520 ‘Development of Nanotechnology-based Biosensors for Agriculture’, Scientific grant of The Research Council of Lithuania (application registration No. VIZ-TYR-126, 2015), by Campus France (PHC GILIBERT 2015, PROJET N° 32978PG and PHC OSMOSE 2016, PROJET N° 35056UB) and by the ANR project ANR-14-CE07-0011 “BONALD”. Z.B., I.B. and A.R. research was funded by a grant (No. TAP LZ-3/2015) from the Research Council of Lithuania. K.Z. acknowledges support from Polish National Science Center Grant DEC-2014/15/B/ST3/02927.

## **REFERENCES**

1. Ozgur, U.; Alivov, Y. I.; Liu, C.; Teke, A.; Reshchikov, M. A.; Dogan, S.; Avrutin, V.; Cho, S. J.; Morkoc, H., A Comprehensive Review of ZnO Materials and Devices. *J. Appl. Phys.* **2005**, *98*, 041301.



2. Bechelany, M.; Amin, A.; Brioude, A.; Cornu, D.; Miele, P., ZnO Nanotubes by Template-Assisted Sol-Gel Route. *J. Nanopart. Res.* **2012**, *14*, 980.
3. Abou Chaaya, A.; Bechelany, M.; Balme, S.; Miele, P., ZnO 1D Nanostructures Designed by Combining Atomic Layer Deposition and Electrospinning for UV Sensor Applications. *J. Mater. Chem. A* **2014**, *2*, 20650-20658.
4. Ahn, M. W.; Park, K. S.; Heo, J. H.; Kim, D. W.; Choi, K. J.; Park, J. G., On-Chip Fabrication of ZnO-Nanowire Gas Sensor with High Gas Sensitivity. *Sens. Actuator B-Chem.* **2009**, *138*, 168-173.
5. Drobek, M.; Kim, J.-H.; Bechelany, M.; Vallicari, C.; Julbe, A.; Kim, S. S., MOF-Based Membrane Encapsulated ZnO Nanowires for Enhanced Gas Sensor Selectivity. *ACS Appl. Mater. Interfaces* **2016**, *8*, 8323-8328.
6. Viter, R.; Khranovskyy, V.; Starodub, N.; Ogorodniichuk, Y.; Gevelyuk, S.; Gertnere, Z.; Poletaev, N.; Yakimova, R.; Erts, D.; Smyntyna, V.; *et al.*, Application of Room Temperature Photoluminescence From ZnO Nanorods for Salmonella Detection. *IEEE Sens. J.* **2014**, *14*, 2028-2034.
7. Tereshchenko, A.; Bechelany, M.; Viter, R.; Khranovskyy, V.; Smyntyna, V.; Starodub, N.; Yakimova, R., Optical Biosensors Based on ZnO Nanostructures: Advantages and Perspectives. A Review. *Sens. Actuator B-Chem.* **2016**, *229*, 664-677.
8. Viter, R.; Abou Chaaya, A.; Iatsunskiy, I.; Nowaczyk, G.; Kovalevskis, K.; Erts, D.; Miele, P.; Smyntyna, V.; Bechelany, M., Tuning of ZnO 1D Nanostructures by Atomic Layer Deposition and Electrospinning for Optical Gas Sensor Applications. *Nanotechnology* **2015**, *26*, 105501.
9. Joshi, B. N.; Yoon, H.; Na, S.-H.; Choi, J.-Y.; Yoon, S. S., Enhanced Photocatalytic Performance of Graphene-ZnO Nanoplatelet Composite Thin Films Prepared by Electrostatic Spray Deposition. *Ceram. Int.* **2014**, *40*, 3647-3654.
10. Mao, S.; Cui, S.; Yu, K.; Wen, Z.; Lu, G.; Chen, J., Ultrafast Hydrogen Sensing Through Hybrids of Semiconducting Single-Walled Carbon Nanotubes and Tin Oxide Nanocrystals. *Nanoscale* **2012**, *4*, 1275-1279.
11. Dutta, M.; Sarkar, S.; Ghosh, T.; Basak, D., ZnO/Graphene Quantum Dot Solid-State Solar Cell. *J. Phys. Chem. C* **2012**, *116*, 20127-20131.
12. Liu, F.; Zhang, Y.; Yu, J.; Wang, S.; Ge, S.; Song, X., Application of ZnO/Graphene and S6 Aptamers for Sensitive Photoelectrochemical Detection of SK-BR-3 Breast Cancer Cells Based on a Disposable Indium Tin Oxide Device. *Biosens. Bioelectron.* **2014**, *51*, 413-420.
13. Son, D. I.; Kwon, B. W.; Park, D. H.; Seo, W.-S.; Yi, Y.; Angadi, B.; Lee, C.-L.; Choi, W. K., Emissive ZnO-Graphene Quantum Dots for White-Light-Emitting Diodes. *Nature Nanotech.* **2012**, *7*, 465-471.
14. Singh, G.; Choudhary, A.; Haranath, D.; Joshi, A. G.; Singh, N.; Singh, S.; Pasricha, R., ZnO Decorated Luminescent Graphene as a Potential Gas Sensor at Room Temperature. *Carbon* **2012**, *50*, 385-394.
15. Wang, C.; Yin, L.; Zhang, L.; Xiang, D.; Gao, R., Metal Oxide Gas Sensors: Sensitivity and Influencing Factors. *Sensors* **2010**, *10*, 2088-2106.
16. Alver, U.; Zhou, W.; Belay, B.; Krueger, R.; Davis, K. O.; Hickman, N. S., Optical and Structural Properties of ZnO Nanorods Grown on Graphene Oxide and Reduced Graphene Oxide Film by Hydrothermal Method. *Appl. Surf. Sci.* **2012**, *258*, 3109-3114.
17. Fay, S.; Shah, A., Zinc Oxide Grown by CVD Process as Transparent Contact for Thin Film Solar Cell Applications. In *Transparent Conductive Zinc Oxide: Basics and Applications in Thin Film Solar Cells*, Ellmer, K.; Klein, A.; Rech, B., Eds. *Springer Berlin Heidelberg: Berlin, Heidelberg*, **2008**, 235-302.

18. Ding, J.; Yan, X.; Xue, Q., Study on Field Emission and Photoluminescence Properties of ZnO/Graphene Hybrids Grown on Si Substrates. *Mater. Chem. Phys.* **2012**, *133*, 405-409.
19. Ismail, A.; Abdullah, M. J., The structural and Optical Properties of ZnO Thin Films Prepared at Different RF Sputtering Power. *J. King Saud Univ. Sci.* **2013**, *25*, 209-215.
20. Ding, J.; Wang, M.; Deng, J.; Gao, W.; Yang, Z.; Ran, C.; Zhang, X., A Comparison Study Between ZnO Nanorods Coated with Graphene Oxide and Reduced Graphene Oxide. *J. Alloy. Comp.* **2014**, *582*, 29-32.
21. Lu, T.; Zhang, Y.; Li, H.; Pan, L.; Li, Y.; Sun, Z., Electrochemical Behaviors of Graphene-ZnO and Graphene-SnO<sub>2</sub> Composite Films for Supercapacitors. *Electrochim. Acta* **2010**, *55*, 4170-4173.
22. Whitby, J. A.; Ostlund, F.; Horvath, P.; Gabureac, M.; Riesterer, J. L.; Utke, I.; Hohl, M.; Sedlacek, L.; Jiruse, J.; Friedli, V.; et al., High Spatial Resolution Time-of-Flight Secondary Ion Mass Spectrometry for the Masses: A Novel Orthogonal ToF FIB-SIMS Instrument with In Situ AFM. *Adv. Mater. Sci. Eng.* **2012**, *2012*, 180437.
23. Abou Chaaya, A.; Viter, R.; Bechelany, M.; Alute, Z.; Erts, D.; Zaleskaya, A.; Kovalevskis, K.; Rouessac, V.; Smyntyna, V.; Miele, P., Evolution of Microstructure and Related Optical Properties of ZnO grown by Atomic Layer Deposition. *Beilstein J. Nanotechnol.* **2013**, *4*, 690-698.
24. George, S. M., Atomic Layer Deposition: An Overview. *Chem. Rev.* **2010**, *110*, 111-131.
25. Hernandez, Y.; Nicolosi, V.; Lotya, M.; Blighe, F. M.; Sun, Z.; De, S.; McGovern, I. T.; Holland, B.; Byrne, M.; et al., High-Yield Production of Graphene by Liquid-Phase Exfoliation of Graphite. *Nature Nanotech.* **2008**, *3*, 563-568.
26. Loryuenyong, V.; Totepvimarn, K.; Eimburanapratvat, P.; Boonchompoo, W.; Buasri, A., Preparation and Characterization of Reduced Graphene Oxide Sheets via Water-Based Exfoliation and Reduction Methods. *Adv. Mater. Sci. Eng.* **2013**, *2013*, 923403.
27. First, P. N.; de Heer, W. A.; Seyller, T.; Berger, C.; Stroscio, J. A.; Moon, J.-S., Epitaxial Graphenes on Silicon Carbide. *MRS Bull.* **2010**, *35*, 296-305.
28. Yao, Y.; Li, Z.; Lin, Z.; Moon, K.-S.; Agar, J.; Wong, C., Controlled Growth of Multilayer, Few-Layer, and Single-Layer Graphene on Metal Substrates. *J. Phys. Chem. C* **2011**, *115*, 5232-5238.
29. Kavitha, T.; Gopalan, A. I.; Lee, K.-P.; Park, S.-Y., Glucose Sensing, Photocatalytic and Antibacterial Properties of Graphene-ZnO Nanoparticle Hybrids. *Carbon* **2012**, *50*, 2994-3000.
30. Jiao, K.; Wu, X.; Duan, C.; Zhang, D.; Wang, Y.; Chen, Y., Novel ALD-Assisted Growth of ZnO Nanorods on Graphene and its Cu<sub>2</sub>ZnSn(S<sub>x</sub>Se<sub>1-x</sub>)<sub>4</sub> Solar Cell Application. *Phys. Chem. Chem. Phys.* **2015**, *17*, 4757-4762.
31. Lin, J.-C.; Huang, B.-R.; Lin, T.-C., Hybrid Structure of Graphene Sheets/ZnO Nanorods for Enhancing Electron Field Emission Properties. *Appl. Surf. Sci.* **2014**, *289*, 384-387.
32. Viter, R.; Iatsunskyi, I.; Fedorenko, V.; Tumenas, S.; Balevicius, Z.; Ramanayicius, A.; Balme, S.; Kempinski, M.; Nowaczyk, G.; Jurga, S.; et al., Enhancement of Electronic and Optical Properties of ZnO/Al<sub>2</sub>O<sub>3</sub> Nanolaminate Coated Electrospun Nanofibers. *J. Phys. Chem. C* **2016**, *120*, 5124-5132.
33. Mattevi, C.; Kim, H.; Chhowalla, M., A Review of Chemical Vapour Deposition of Graphene on Copper. *J. Mater. Chem.* **2011**, *21*, 3324-3334.
34. Ghoneim, M. T.; Smith, C. E.; Hussain, M. M., Simplistic Graphene Transfer Process and its Impact on Contact Resistance. *Appl. Phys. Lett.* **2013**, *102*, 183115.

35. Bachmann, J.; Zierold, R.; Chong, Y. T.; Hauert, R.; Sturm, C.; Schmidt-Grund, R.; Rheinlaender, B.; Grundmann, M.; Goesele, U.; Nielsch, K., A Practical, Self-catalytic, Atomic Layer Deposition of Silicon Dioxide. *Angew. Chem. Int. Ed.* **2008**, *47*, 6177-6179.
36. Iatsunskiy, I.; Coy, E.; Viter, R.; Nowaczyk, G.; Jancelewicz, M.; Baleviciute, I.; Zaleski, K.; Jurga, S., Study on Structural, Mechanical, and Optical Properties of Al<sub>2</sub>O<sub>3</sub>-TiO<sub>2</sub> Nanolaminates Prepared by Atomic Layer Deposition. *J. Phys. Chem. C* **2015**, *119*, 20591-20599.
37. Hybertsen, M. S.; Louie, S. G., First-Principles Theory for the Quasiparticle Energies of Semiconductors and Insulators. *Phys. Rev. Lett.* **1985**, *55*, 1418-1421.
38. Klingshirn, C., Introduction. In Zinc Oxide: From Fundamental Properties Towards Novel Applications, *Springer Berlin Heidelberg: Berlin, Heidelberg*, **2010**, 1-6.
39. Xu, P.; Tang, Q.; Zhou, Z., Structural and Electronic Properties of Graphene-ZnO Interfaces: Dispersion-Corrected Density Functional Theory Investigations. *Nanotechnology* **2013**, *24*, 305401.
40. Stoev, K.; Sakurai, K., Recent Theoretical Models in Grazing Incidence X-ray Reflectometry. *Rigaku J.* **1997**, *14*, 22-37.
41. Seo, T. H.; Lee, S.; Cho, H.; Chandramohan, S.; Suh, E.-K.; Lee, H. S.; Bae, S. K.; Kim, S. M.; Park, M.; Lee, J. K.; Kim, M. J., Tailored CVD Graphene Coating as a Transparent and Flexible Gas Barrier. *Sci. Rep.* **2016**, *6*, 24143.
42. Malard, L. M.; Pimenta, M. A.; Dresselhaus, G.; Dresselhaus, M. S., Raman Spectroscopy in Graphene. *Phys. Rep.* **2009**, *473*, 51-87.
43. Kudin, K. N.; Ozbas, B.; Schniepp, H. C.; Prud'homme, R. K.; Aksay, I. A.; Car, R., Raman Spectra of Graphite Oxide and Functionalized Graphene Sheets. *Nano Lett.* **2008**, *8*, 36-41.
44. Wu, W.; Yu, Q.; Peng, P.; Liu, Z.; Bao, J.; Pei, S.-S., Control of Thickness Uniformity and Grain Size in Graphene Films for Transparent Conductive Electrodes. *Nanotechnology* **2012**, *23*, 035603.
45. Luo, Z.; Lu, Y.; Singer, D. W.; Berck, M. E.; Somers, L. A.; Goldsmith, B. R.; Johnson, A. T. C., Effect of Substrate Roughness and Feedstock Concentration on Growth of Wafer-Scale Graphene at Atmospheric Pressure. *Chem. Mater.* **2011**, *23*, 1441-1447.
46. Shin, K.-S.; Jo, H.; Shin, H.-J.; Choi, W. M.; Choi, J.-Y.; Kim, S.-W., High Quality Graphene-Semiconducting Oxide Heterostructure for Inverted Organic Photovoltaics. *J. Mater. Chem.* **2012**, *22*, 13032-13038.
47. Beams, R.; Cancado, L. G.; Novotny, L., Raman Characterization of Defects and Dopants in Graphene. *J. Phys. Condens. Matter* **2015**, *27*, 083002.
48. Si, C.; Sun, Z.; Liu, F., Strain Engineering of Graphene: a Review. *Nanoscale* **2016**, *8*, 3207-3217.
49. Iqbal, M. W.; Iqbal, M. Z.; Khan, M. F.; Jin, X.; Hwang, C.; Eom, J., Modification of the Structural and Electrical Properties of Graphene Layers by Pt Adsorbates. *Sci. Technol. Adv. Mater.* **2014**, *15*, 055002.
50. Abou Chaaya, A.; Viter, R.; Baleviciute, I.; Bechelany, M.; Ramanavicius, A.; Gertner, Z.; Erts, D.; Smyntyna, V.; Miele, P., Tuning Optical Properties of Al<sub>2</sub>O<sub>3</sub>/ZnO Nanolaminates Synthesized by Atomic Layer Deposition. *J. Phys. Chem. C* **2014**, *118*, 3811-3819.
51. Ozerov, I.; Arab, M.; Safarov, V. I.; Marine, W.; Giorgio, S.; Sentis, M.; Nanai, L., Enhancement of Exciton Emission from ZnO Nanocrystalline Films by Pulsed Laser Annealing. *Appl. Surf. Sci.* **2004**, *226*, 242-248.
52. Reynolds, D. C.; Look, D. C.; Jogai, B.; Collins, T. C., Polariton and Free-Exciton-Like Photoluminescence in ZnO. *Appl. Phys. Lett.* **2001**, *79*, 3794-3796.

53. Raghavan, R.; Bechelany, M.; Parlinska, M.; Frey, D.; Mook, W. M.; Beyer, A.; Michler, J.; Utke, I., Nanocrystalline-to-Amorphous Transition in Nanolaminates Grown by Low Temperature Atomic Layer Deposition and Related Mechanical Properties. *Appl. Phys. Lett.* **2012**, *100*, 191912.
54. Viter, R.; Baleviciute, I.; Abou Chaaya, A.; Mikoliunaite, L.; Balevicius, Z.; Ramanavicius, A.; Zalesska, A.; Vatamana, V.; Smyntyna, V.; Gertnere, et al., Optical Properties of Ultrathin Al<sub>2</sub>O<sub>3</sub>/ZnO Nanolaminates. *Thin Solid Films* **2015**, *594*, 96-100.
55. Chang, Y.-C.; Liu, C.-H.; Liu, C.-H.; Zhang, S.; Marder, S. R.; Narimanov, E. E.; Zhong, Z.; Norris, T. B., Realization of Mid-infrared Graphene Hyperbolic Metamaterials. *Nat Commun.* **2016**, *7*, 10568.
56. Seo, H.-K.; Park, M.-H.; Kim, Y.-H.; Kwon, S.-J.; Jeong, S.-H.; Lee, T.-W., Laminated Graphene Films for Flexible Transparent Thin Film Encapsulation. *ACS Appl. Mater. Interfaces* **2016**, *8*, 14725-14731.
57. Malekpour, H.; Chang, K. H.; Chen, J. C.; Lu, C. Y.; Nika, D. L.; Novoselov, K. S.; Balandin, A. A., Thermal Conductivity of Graphene Laminate. *Nano Lett.* **2014**, *14*, 5155-5161.

## FIGURES

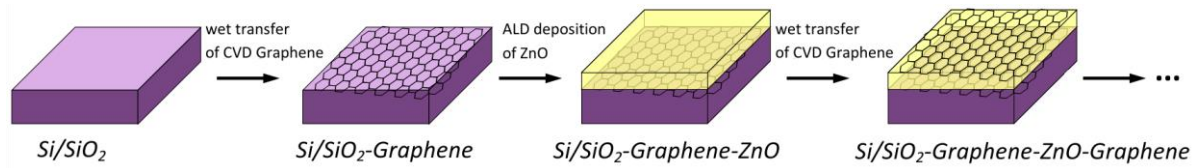


**Figure 1.** Schematic representation of fabrication of G/ZnO nanolaminates by alternating ZnO deposition and graphene transfer.

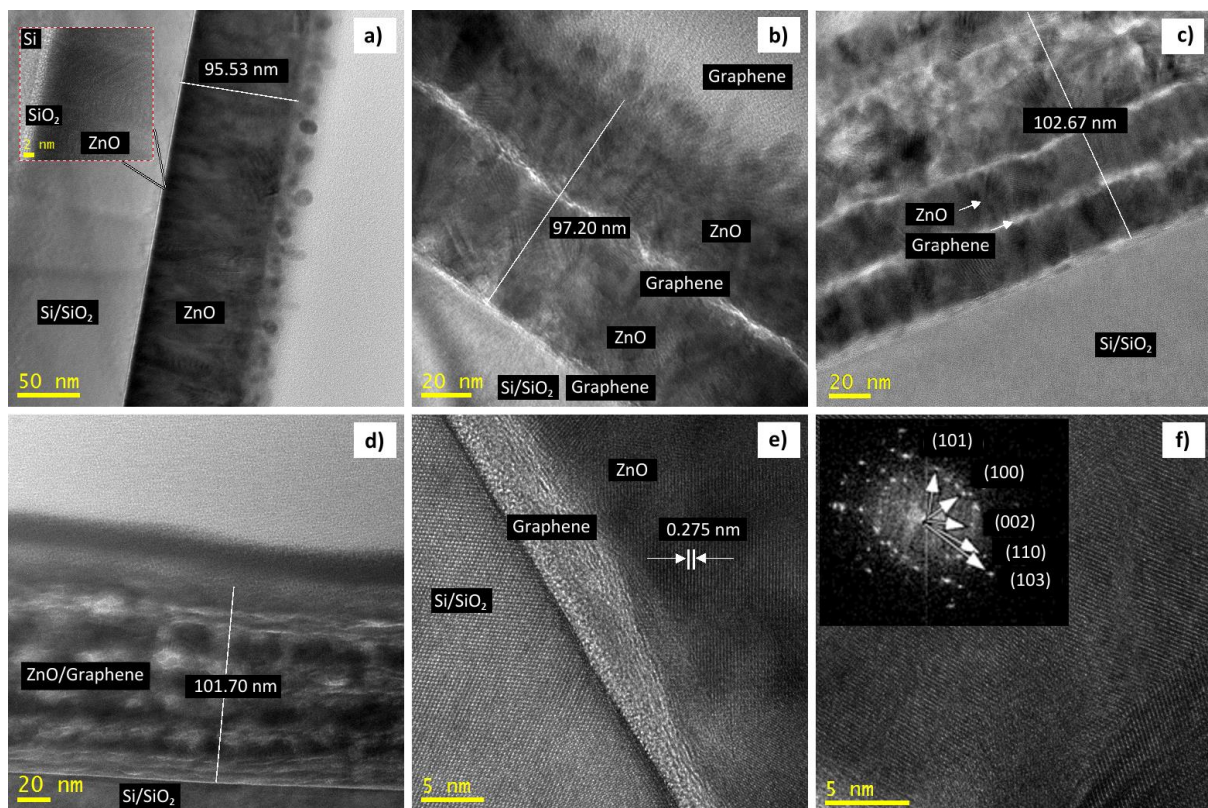


**Figure 2.** TEM images of cross-section of pure ZnO layer (a) and Graphene/ZnO nanolaminates with different number of graphene layers: b)  $G_{3L}ZnO_{50nm}$ , c)  $G_{5L}ZnO_{25nm}$ , d)  $G_{11L}ZnO_{10nm}$ , (e) interface of  $\text{Si/SiO}_2$ -Graphene-ZnO, f) interlayer of ZnO of the sample  $G_{11L}ZnO_{10nm}$  and FFT of this area.

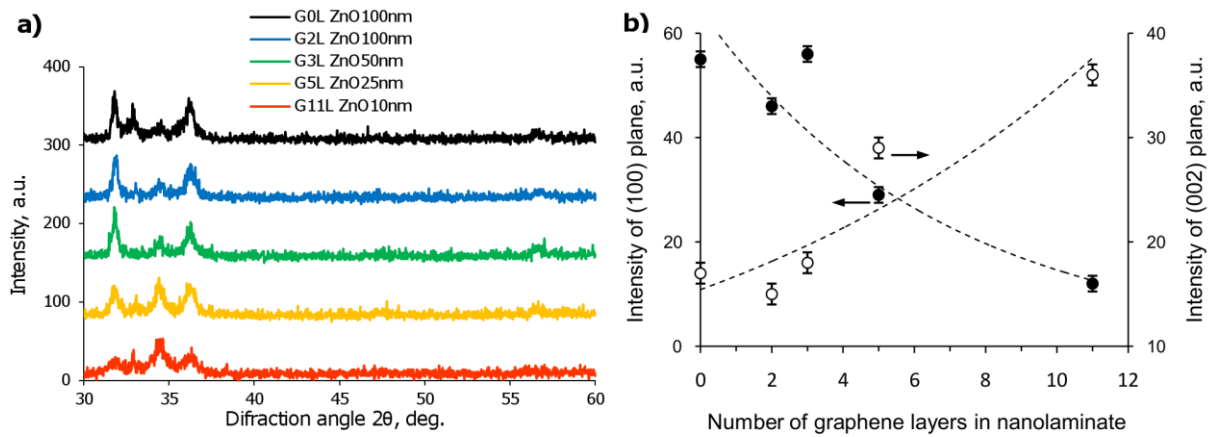


**Figure 3.** X-ray diffraction patterns of ZnO thin film and Graphene/ZnO nanolaminates (a) and curves illustrating intensities of diffraction peaks of (100) plane (closed symbols, primary scale) and of (002) plane (open symbols, secondary scale) vs number of graphene layers in the G/ZnO nanolaminates (b)

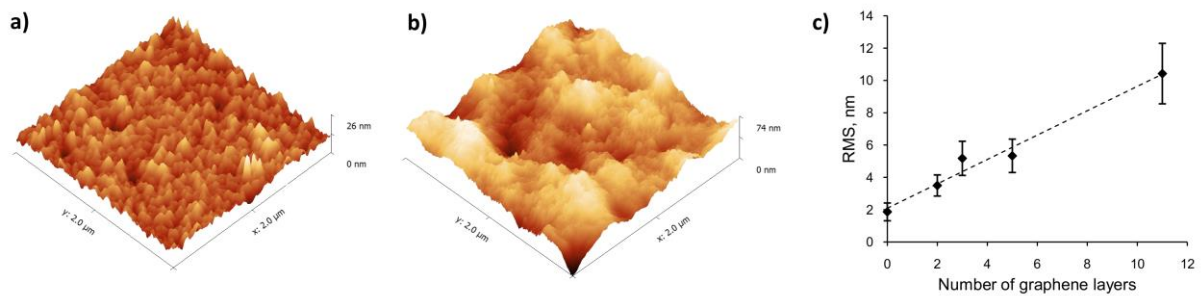


**Figure 4.** AFM images of the surface of Graphene/ZnO nanolaminates with 2 graphene layers: G<sub>2</sub>LZnO<sub>100nm</sub> (a), with 11 graphene layers G<sub>11</sub>LZnO<sub>10nm</sub> (b) and the dependence of number of graphene layers to surface roughness of 100 nm thick Graphene/ZnO nanolaminates (c).

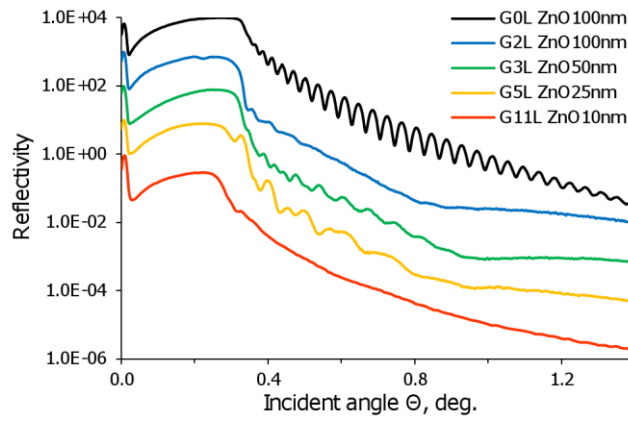


**Figure 5.** X-ray reflectivity profiles of ZnO thin film and Graphene/ZnO nanolaminates.

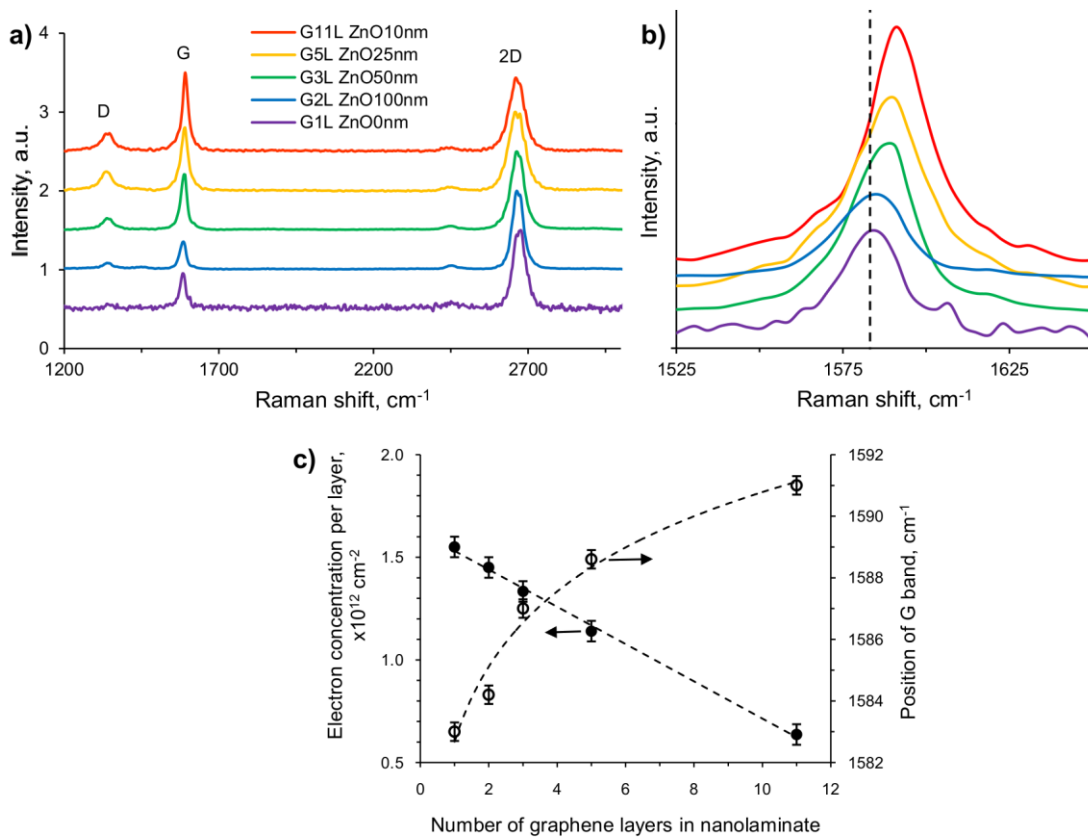


**Figure 6.** Raman spectra of graphene and Graphene/ZnO nanolaminates (a), close view of G band shifting (b), and curves illustrating shifting of G band (open symbols, secondary scale) and charge per graphene layer (closed symbols, primary scale) vs number of graphene layers in the G/ZnO nanolaminates (c)



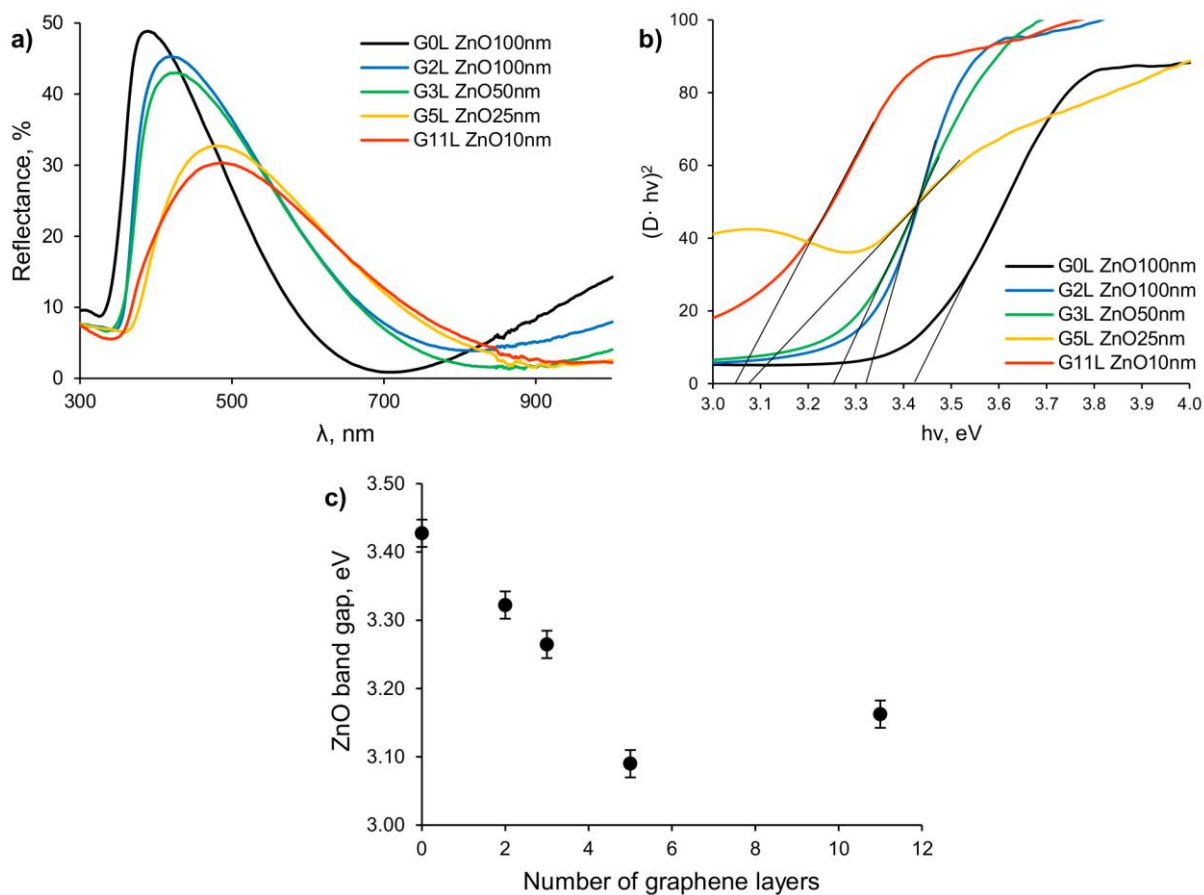


**Figure 7.** Reflectance spectra (a), band gap calculation on the absorption edge from reflectance spectra (b) and dependence of the ZnO band gap on the number of graphene layers (c) of ZnO thin film and Graphene/ZnO nanolaminates.

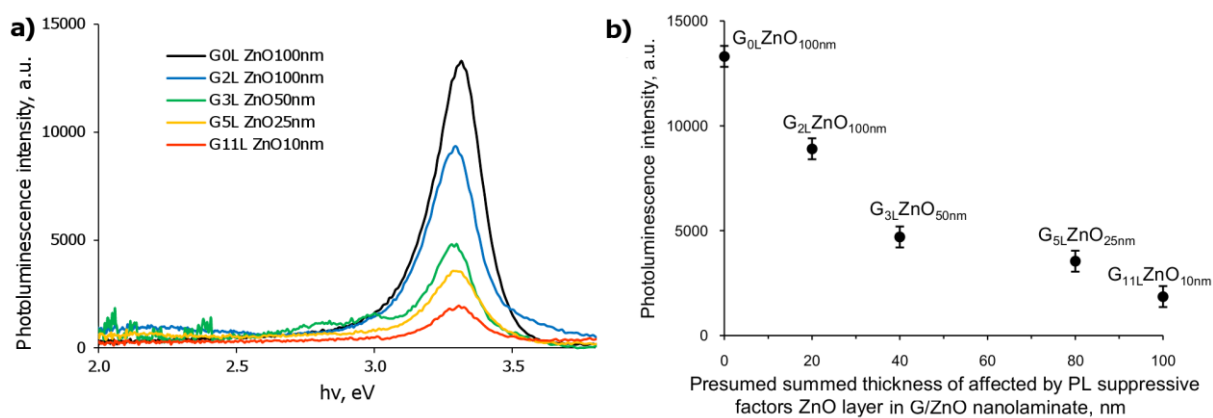


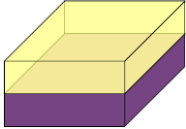
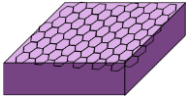
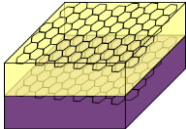
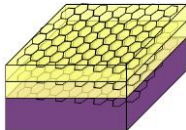
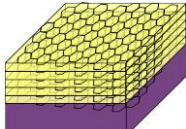
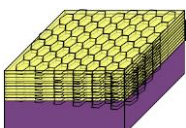
**Figure 8.** Photoluminescence spectra of ZnO thin film and Graphene/ZnO nanolaminates (a), Graphene/ZnO nanolaminate photoluminescence intensity vs. presumed summed thickness of



*ZnO layer affected by PL suppressive factors in G/ZnO (calculated assuming 10 nm thick ZnO layers affected by PL suppressive factors near the every surface of individual graphene layers).*

## TABLES

**Table 1.** Ratio of bands intensities of single graphene layer and Graphene/ZnO nanolaminates calculated from Raman spectra; Measurement deviation is calculated from the TEM images.

Sample	Schematic representation	Thickness of each interlayer (nm)	Number of ZnO layers	Number of graphene layers	Number of ZnO layers	$I_{2D}/I_G$	$I_D/I_G$
G <sub>0</sub> LZnO <sub>100nm</sub>		100±5	0	1	1	-	-
G <sub>1</sub> LZnO <sub>0nm</sub>		-	1	0	0	2.18	0.1
G <sub>2</sub> LZnO <sub>100nm</sub>		100±5	2	1	1	2.68	0.22
G <sub>3</sub> LZnO <sub>50nm</sub>		50±1.4	3	2	2	1.33	0.20
G <sub>5</sub> LZnO <sub>25nm</sub>		25±0.5	5	4	4	1.20	0.24
G <sub>11</sub> LZnO <sub>10nm</sub>		10±0.3	11	10	10	0.87	0.21

## TOC FIGURE

